14-3-3ε UFMylation promotes RIG-I-mediated signaling

Isaura Vanessa Gutierrez[1], Moonhee Park[1], Lauren Sar[1], Ryan Rodriguez[2], Daltry L. Snider[2], Gabriella Torres[1], K. Matthew Scaglione[2,3], Stacy M. Horner[1,2,4]

[1] Department of Integrative Immunobiology, Duke University School of Medicine, Durham, NC, USA

[2] Department of Molecular Genetics and Microbiology, Duke University School of Medicine, Durham, NC, USA

[3] Duke Center for Neurodegeneration and Neurotherapeutics, Duke University School of Medicine, Durham, NC, USA

[4] Department of Medicine, Duke University School of Medicine, Durham, NC, USA

Correspondence: stacy.horner@duke.edu
Stacy M. Horner, Ph.D.
Duke University School of Medicine
213 Research Dr., Box 3053 DUMC
Durham, NC USA 27710
Phone: 919-684-1921

Abstract

Post-translational modifications are critical for regulating the RIG-I signaling pathway. Previously, we identified a role for the post-translation modification UFM1 (UFMylation) in promoting RIG-I signaling by stimulating the interaction between RIG-I and its membrane-targeting protein 14-3-3ε. Here, we identify UFMylation of 14-3-3ε as a novel regulatory mechanism promoting RIG-I signaling. We demonstrate that UFM1 conjugation to lysine residue K50 or K215 results in mono-UFMylation on 14-3-3ε and enhances its ability to promote RIG-I signaling. Importantly, we show that mutation of these residues (K50R/K215R) abolishes UFMylation and impairs induction of type I and III interferons without disrupting the interaction between 14-3-3ε and RIG-I. This suggests that UFMylation of 14-3-3ε likely stabilizes signaling events downstream of RIG-I activation to promote induction of interferon. Collectively, our work suggests that UFMylation-driven activation of 14-3-3ε facilitates innate immune signaling and highlights the broader role of UFMylation for antiviral defense and immune regulation.

Importance

Post-translational modifications provide regulatory control of antiviral innate immune responses. Our study reveals that UFMylation of 14-3-3ε is a control point for RIG-I-mediated antiviral signaling. We demonstrate that conjugation of UFM1 to specific lysine residues on 14-3-3ε enhances downstream signaling events that facilitate interferon induction, but surprisingly it does not affect 14-3-3ε binding to RIG-I. By identifying the precise sites of UFMylation on 14-3-3ε and their functional consequences, we provide insights into the regulatory layers governing antiviral innate immunity. These findings complement emerging evidence that UFMylation serves as a versatile modulator across diverse immune pathways. Furthermore, our work highlights how protein chaperones like 14-3-3ε can be dynamically modified to orchestrate complex signaling cascades, suggesting potential therapeutic approaches for targeting dysregulated innate immunity.

Introduction

The antiviral innate immune response is tightly regulated to ensure effective defense against viral infections while preventing excessive inflammation. This antiviral response to RNA viruses is activated by cytosolic RIG-I-like receptors (RLRs) RIG-I and MDA5, which detect pathogen-associated molecular patterns from RNA viruses and initiate the formation of a MAVS-signaling complex (1). This complex activates a downstream signaling cascade that leads to the transcriptional activation of type I and type III interferons (IFN) and the production of IFN-stimulated genes (ISGs) that limit viral replication. Robust innate immune signaling is essential for effective adaptive immunity, but dysregulation of these pathways can result in autoimmune diseases and interferonopathies (2-4). Therefore, the induction of IFN is carefully regulated by mechanisms that temporarily activate, dampen, and ultimately shut down the signaling pathway.

Both 14-3-3ε and 14-3-3η are examples of RLR regulatory proteins that regulate IFN induction. These proteins facilitate the translocation of RIG-I and MDA5, respectively, from the cytosol to intracellular membrane signaling sites to interact with MAVS (5, 6). 14-3-3 proteins are highly conserved regulatory molecules involved in diverse cellular processes, including signal transduction, apoptosis, and stress responses. Typically, they regulate cellular processes by binding to phosphorylated client proteins, although they are also known to bind to non-phosphorylated client proteins, including those containing other post-translational modifications (PTMs) beyond phosphorylation (7-13). Recent work has also suggested that 14-3-3 proteins can serve as protein chaperones, preventing aggregation and phase separation of their client proteins (14). Orthoflavivirus NS3 proteins specifically target and inactivate both 14-3-3ε and 14-3-3η to prevent RLR signaling, and the enterovirus 3C protease cleaves 14-3-3ε, underscoring the essential role of these membrane-targeting proteins in antiviral innate immunity (15-17).

Post-translational modifications play a crucial role in regulating RIG-I signaling (18, 19). Recent studies by our group have shown that ubiquitin-fold modifier 1 (UFM1) and the proteins involved in UFM1 conjugation promote RIG-I signaling (20). UFMylation involves the covalent conjugation of ubiquitin-fold modifier 1 (UFM1), an 85-amino acid peptide, to lysine residues on proteins, utilizing an E1 activating enzyme (UBA5), an E2 conjugating enzyme (UFC1), and an E3 scaffold-like ligase complex (UFL1 and the membrane-anchored protein UFBP1) (21-29). UFM1 is a non-degradative mark, and its addition to proteins can alter their interactions. UFMylation modulates various cellular processes, including the DNA damage response and genomic instability, various aspects of ER homeostasis and translation, ER-Golgi transport, viral infection, cancer progression, and both adaptive and innate immune responses (23, 24, 26, 27, 30-43). For example, UFMylation of the ribosomal protein RPL26 enhances hepatitis A virus

translation (44). In orthoflaviviruses, UFMylation promotes the production of infectious virions (45). Interestingly, viruses have evolved mechanisms to manipulate host UFMylation pathways by targeting UFL1 to specific substrates. For example, orthoflaviviruses co-opt UFL1 to aid in viral assembly (45), while Epstein-Barr virus (EBV) targets UFL1 to MAVS for UFMylation to dampen inflammasome activation (46). Others have shown that UFMylation promotes NLRP3 activation or that it can limit LPS-mediated inflammation via its roles in regulating ER homeostasis and the unfolded protein response (47-51). UFL1 can also bind STING during HSV-1 infection to maintain IFN induction (52). Thus, UFL1 or UFMylation can influence viral infection and innate immune responses in diverse ways.

Our previous work on UFMylation in the context of RIG-I signaling revealed that UFL1 translocates to intracellular membranes upon RIG-I activation (20, 53). We identified roles for UFL1 and UFM1 in facilitating RIG-I interaction with 14-3-3ε and found that 14-3-3ε exhibits increased UFMylation in response to RIG-I activation. However, several critical questions remained unanswered. First, does UFMylation directly modulate 14-3-3ε function during RIG-I signaling? Second, which specific lysine residues on 14-3-3ε serve as UFMylation sites? Third, how does UFMylation functionally impact 14-3-3ε's role in RIG-I-mediated signaling? We hypothesized that direct UFMylation of 14-3-3ε at specific lysine residues enhances its ability to promote RIG-I signaling. Here, we demonstrate that UFM1 conjugation enhances 14-3-3ε-mediated RIG-I signaling. We then identify lysine residues on 14-3-3ε that are UFMylated. Then, we show how UFMylation of these lysine residues regulates RIG-I-dependent IFN induction

Results

UFM1 conjugation is required to promote 14-3-3ε-mediated enhancement of RIG-I signaling to IFN-β. To determine whether UFM1 plays a functional role in enhancing RIG-I signaling through 14-3-3ε, we first assessed its effect on IFN-β promoter activation**.** Using IFN-β promoter luciferase assays in 293T cells, we found that ectopic expression of UFM1 significantly enhanced RIG-I driven signaling to IFN-β. This signaling was further amplified when UFM1 was co-expressed with both RIG-I and 14-3-3ε, suggesting these three proteins cooperate for signaling regulation (Figure 1A). Next, to determine whether the conjugation of UFM1 is specifically required for this enhancement, we generated a conjugation-deficient UFM1 mutant (ΔC3) by deleting three amino acids from its C-terminus to prevent covalent attachment of UFM1 to target proteins (21). Using IFN-β promoter luciferase assays in 293T cells, we found that unlike wild-type UFM1, the conjugation-deficient UFM1 mutant failed to enhance 14-3-3ε-driven RIG-I

116 signaling (Figure 1B). These results demonstrate that UFM1 must be covalently conjugated to
117 proteins to facilitate 14-3-3ε-mediated enhancement of RIG-I signaling to the IFN-β promoter.
118
119 **UFM1 conjugation to 14-3-3ε requires residues K50 and K215 on 14-3-3ε.** Having established
120 that UFM1 conjugation is required for 14-3-3ε-mediated enhancement of RIG-I signaling, we next
121 sought to verify our previous results that 14-3-3ε is directly UFMylated (20) and determine which
122 specific lysine residues serve as UFM1-conjugation sites. First, we wanted to verify 14-3-3ε
123 UFMylation in cells. For this, we developed a modified UFMylation assay based on previous
124 studies (54). In this assay, we co-expressed HA-tagged 14-3-3ε, Flag-UFM1, and the UFMylation
125 ligase complex proteins UFL1 and UFBP1 in 293T-UFM1 KO cells generated by CRISPR/Cas9
126 targeting. Critically, lysates were boiled prior to immunoprecipitation to denature protein
127 complexes, ensuring that only proteins covalently linked to the immunoprecipitated protein would
128 be detected in subsequent analyses. Following HA-immunoprecipitation, we identified a single
129 Flag-UFM1 conjugation to 14-3-3ε, consistent with a mono-UFMylation event (Figure 2A).
130 Importantly, the conjugation-deficient Flag-UFM1-ΔC3 showed no attachment of 14-3-3ε, while a
131 deconjugation-resistant Flag-UFM1-G83A mutant (21) demonstrated significantly increased
132 levels of 14-3-3ε UFMylation.
133 Having established that UFM1 conjugation is required for RIG-I signaling, we next sought
134 to identify the specific lysine residues on 14-3-3ε that undergo UFMylation by using mass
135 spectrometry analysis. We used Huh7 cells stably expressing Flag-UFM1 with a two amino acid
136 deletion (ΔC2) that enhances detection of UFMylated proteins by eliminating the prerequisite of
137 G-SC cleavage in UFM1 by the UFSP1/UFSP2 proteins that needs to occur to initiate the
138 UFMylation pathway (21). After HA-immunoprecipitation of HA-tagged 14-3-3ε, mass
139 spectrometry analysis identified three peptides containing two lysine residues, K50 and K215,
140 that were covalently modified by UFM1. Both K50 and K215 reside within clusters of basic
141 residues within a positively charged pocket of the conserved amphipathic ligand binding groove
142 of 14-3-3 proteins.
143 To confirm these specific sites as bona fide UFMylation targets, we employed both *in vitro*
144 and cellular UFMylation assays. Using an *in vitro* UFMylation assay with purified UFMylation
145 proteins, we demonstrated that wild-type 14-3-3ε has mono-UFMylation, whereas lysine-to-
146 arginine mutations at K50 and K215 (K50R/K215R) abolished this mono-UFMylation (Figure 2B).
147 Similarly, in our cellular UFMylation assay, the K50R-K215R mutations significantly abrogated
148 14-3-3ε mono-UFMylation (Figure 2C). These complementary approaches confirm that K50 and
149 K215 are the principal sites for UFM1 conjugation to 14-3-3ε. However, as we only detect mono-

150 UFMylation of 14-3-3ε, these results also suggest that either K50 or K215 undergo UFM1-
151 conjugation in a molecule of 14-3-3ε.
152
153 **K50 and K215 are not required for 14-3-3ε interaction with RIG-I.** Based on our previous
154 findings that both UFM1 and UFL1 are important for the interaction of RIG-I with 14-3-3ε (20), we
155 hypothesized that UFMylation of 14-3-3ε at either K50 or K215 would be required for its interaction
156 with RIG-I. To test this hypothesis, we performed co-immunoprecipitation experiments comparing
157 RIG-I binding between 14-3-3ε^{WT} or the UFMylation-deficient 14-3-3ε$^{K50/215R}$ mutant.
158 Unexpectedly, we found that 14-3-3ε$^{K50/215R}$ maintained interaction with RIG-I at levels
159 comparable to the wild-type protein (Figure 3A-B), indicating that UFMylation at these residues is
160 not essential for the association of 14-3-3ε and RIG-I. To validate our experimental approach, we
161 included a control mutant of 14-3-3ε where key residues in the C-terminal end (EDE to AAA) were
162 altered, as these previously have been reported to mediate this interaction (55). As expected, this
163 control mutant showed significantly reduced RIG-I binding, confirming the work of others and the
164 specificity of our assay. These results revealed that UFMylation at K50 or K215 are not critical for
165 the interaction between 14-3-3ε and RIG-I.
166
167 **K50 and K215 are required for 14-3-3ε-mediated RIG-I activation of IFN.** Since UFMylation
168 did not affect the binding of for 14-3-3ε to RIG-I, we next investigated whether the K50/K215
169 residues nevertheless impact the ability of 14-3-3ε to enhance RIG-I-mediated signaling using
170 two complementary approaches. First, we evaluated IFN-β promoter activation using a luciferase
171 reporter assay in 293T-RIG-I KO cells. We ectopically expressed 14-3-3ε^{WT} or 14-3-3ε$^{K50/215R}$,
172 along with RIG-I, and measured luciferase activity. While 14-3-3ε^{WT} significantly increased RIG-I
173 signaling to the IFN-β promoter as expected, 14-3-3ε$^{K50/215R}$ showed significantly impaired ability
174 to enhance this signaling (Figure 4A). This result suggests that UFMylation at K50 or K215 is
175 critical for 14-3-3ε to promote RIG-I-mediated transcriptional activation. To directly confirm this
176 finding at the transcriptional level, we measured the induction of endogenous IFN genes by RT-
177 qPCR in response to infection by Sendai virus, a potent activator of RIG-I signaling (56, 57). We
178 ectopically expressed 14-3-3ε^{WT} or 14-3-3ε$^{K50/215R}$, along with RIG-I in 293T-RIG-I KO cells and
179 analyzed the levels of *IFNB1* and *IFNL1* transcripts. Consistent with our luciferase assay results,
180 14-3-3ε$^{K50/215R}$ significantly limited RIG-I-mediated induction of both *IFNB1* and *IFNL1* compared
181 to 14-3-3ε^{WT} (Figure 4B-C). Collectively, these findings demonstrate that while lysine residues
182 required for 14-3-3ε UFMylation do not affect RIG-I binding, they are nevertheless critical for
183 promoting RIG-I-mediated transcriptional activation of type I and type III IFNs, suggesting that

184 UFMylation of 14-3-3ε at K50 and K215 enhances downstream signaling events following initial
185 RIG-I binding.
186
187 **Discussion.**
188 Our study identifies UFMylation of 14-3-3ε as a novel regulatory mechanism that promotes
189 RIG-I-mediated antiviral signaling. Through a series of biochemical and functional analyses, we
190 have demonstrated that UFM1 is covalently conjugated to lysine residues K50 or K215 on 14-3-
191 3ε, and that this modification is critical for 14-3-3ε to enhance RIG-I-dependent IFN induction.
192 Upon viral RNA recognition, activated RIG-I must translocate from the cytosol to intracellular
193 membranes to interact with MAVS within a specialized signaling complex termed the "RIG-I
194 translocon," which includes the K63 ubiquitin ligases TRIM25 and Riplet. One of our most
195 intriguing findings was that mutation of the UFMylation sites (K50R/K215R) abolished the ability
196 of 14-3-3ε to enhance RIG-I signaling without disrupting their physical interaction. This
197 unexpected result suggests that UFMylation modulates 14-3-3ε function through mechanisms
198 beyond simple binding affinity regulation.
199 Previously, we demonstrated that the UFMylation E3 ligase complex member UFL1 is
200 recruited to ER-mitochondrial contact sites following RIG-I activation (20, 53). Our current work
201 extends this model by identifying UFMylation sites on 14-3-3ε (K50 and K215) that are critical for
202 its function in this pathway. The mechanism by which UFMylation enhances 14-3-3ε function may
203 involve electrostatic or conformational changes within its ligand-binding groove as the negative
204 charge of UFM1 in the presence of these positively charged residues is likely to influence how
205 14-3-3ε interacts with and coordinates protein partners at membrane signaling sites (14).
206 Interestingly, our results suggest that only mono-UFMylation occurs on 14-3-3ε. As K50 and K215
207 can reside on opposite faces within the conserved amphipathic ligand-binding groove of 14-3-3ε
208 when 14-3-3ε binds non-phosphorylated proteins, it seems possible that only one site can be
209 UFMylated on any given molecule (10). While the exact function of UFM1-conjugation on 14-3-
210 3ε is still unclear, it may play a role in coordinating multiple protein partners at membrane signaling
211 sites, potentially including known interactors such as Riplet, TRIM25, or MAVS, whose binding to
212 14-3-3ε might be modulated by its UFMylation status. This model aligns with observations in other
213 systems where UFMylation has been shown to serve as a scaffold for optimizing signaling
214 complex organization (40), suggesting a similar role in RIG-I signaling.
215 Our results highlight the sophisticated regulation of 14-3-3 proteins through various PTMs.
216 Interestingly, K50 on 14-3-3ε can be acetylated and sumoylated (58, 59), and this residue in other
217 14-3-3 proteins has been shown to be ubiquitinated (8). This suggests that competing PTMs at

218 the same residue could mediate context-dependent functional switching between distinct cellular
219 pathways. Recent studies have also revealed intrinsic chaperone-like activities for 14-3-3 proteins
220 that broadly prevent aggregation or aberrant phase separation of client proteins (14). We
221 speculate that UFMylation could also enhance these intrinsic chaperone functions of 14-3-3
222 proteins during antiviral responses by stabilizing protein complexes critical to innate immune
223 signaling. This could explain how UFMylation promotes RIG-I signaling without affecting direct
224 binding interactions, by optimizing the molecular environment around the signaling complex
225 rather than altering binding interfaces directly. Future studies will be needed to investigate the
226 molecular events triggering site-specific UFMylation of 14-3-3 following RIG-I activation and to
227 determine whether other 14-3-3 isoforms undergo similar regulation.
228 In summary, by identifying K50 and K215 on 14-3-3ε as a critical target residues of
229 UFMylation that promote RIG-I signaling, our study reveals another mechanism for how this post-
230 translational modification system tunes diverse innate immune pathways, advancing our
231 fundamental understanding of innate immune regulation. The UFMylation pathway represents a
232 potential target for modulating antiviral responses in conditions characterized by either insufficient
233 immunity or excessive inflammation. Furthermore, as viruses have evolved mechanisms to
234 manipulate UFMylation, targeting this pathway could potentially disrupt various aspects of viral
235 infection. Future investigations of UFMylation in both infectious and inflammatory diseases may
236 yield important insights for developing novel immunomodulatory approaches.
237
238 **Acknowledgements**
239 We thank those colleagues who generously provided reagents, as indicated in the Methods, the
240 Duke Functional Genomics Core, the Duke Proteomics and Metabolomics Core Facility, and
241 members of the Horner Lab for valuable feedback and discussion. During the preparation of this
242 work, we used Perplexity for editing purposes. After using this tool/service, we reviewed and
243 sometimes made edits to our text. We take full responsibility for the content of the publication.
244 This work was supported by National Institutes of Health grants R01AI155512 (S.M.H),
245 R35GM119544 (K.M.S), and T32CA00911 (IVG; DLS).
246

247 **Figures**

248

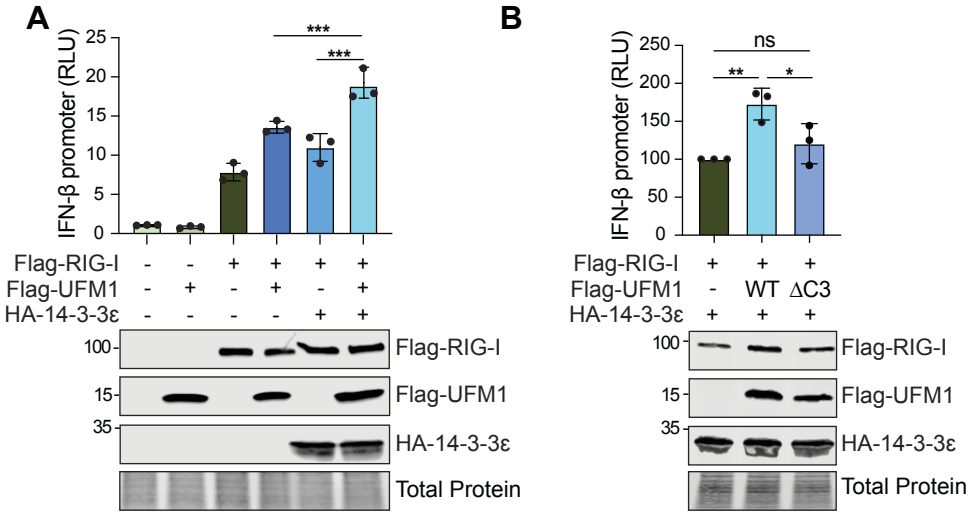

249

250

251 **Figure 1. UFM1 conjugation is required to promote 14-3-3ε-mediated enhancement of RIG-**
252 **I signaling to IFN-β.** (A) IFN-β-promoter reporter luciferase expression (relative to *Renilla)* from
253 293T cells expressing (Vec) Vector, Flag-UFM1^{WT}, Flag-RIG-I, or HA-14-3-3ε. (B) IFN-β–
254 promoter reporter luciferase expression (relative to *Renilla*) from 293T cells expressing (Vec)
255 Vector, Flag-UFM1^{WT}, Flag-UFM1$^{\Delta C3}$, Flag-RIG-I, or HA-14-3-3ε. Bars represent the mean ± SD,
256 $n = 3$ independent replicates. *p ≤ 0.05, ** ≤ 0.01, ***p ≤ 0.001 determined by one way ANOVA
257 followed by Šidák's multiple comparisons test (A) or Tukey's multiple comparisons test (B).

258

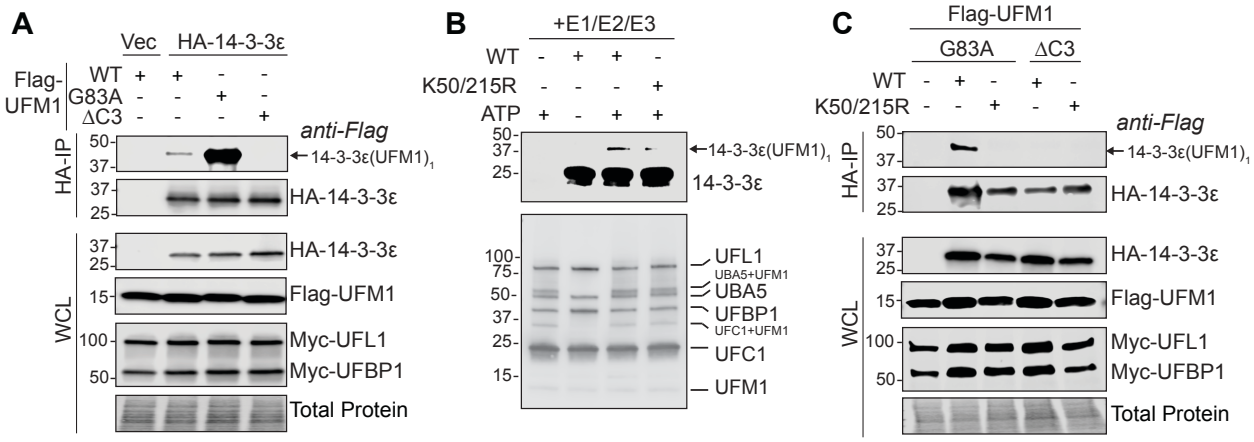

Figure 2. UFM1 conjugation to 14-3-3ε requires residues K50 and K215 on 14-3-3ε. (A) UFMylation assay of anti-HA immunoprecipitated lysates from 293T UFM1 KO cells expressing Vector (Vec) or HA-14-3-3ε along with Myc-UFL1, Myc-UFBP1, and Flag-UFM1-WT, -G83A, or -ΔC3. (B) Purified UFMylation proteins (UFBP1, UFL1, UFC1, UBA5, and UFM1) as well as 14-3-3ε^{WT} or 14-3-3ε$^{K50/215R}$ were incubated in UFMylation assay buffer in the presence or absence of ATP. Following reaction termination, the samples were subjected to immunoblot analysis for 14-3-3ε (top) or using an antibody cocktail to all UFMylation proteins (bottom). (C) UFMylation assay of anti-HA immunoprecipitated lysates from 293T UFM1 KO cells expressing Vector (-), Flag-UFM1-WT, -G83A, or -ΔC3, and HA-14-3-3ε^{WT} or HA-14-3-3ε$^{K50/215R}$. Representative blots from *n* = 3 independent replicates are shown.

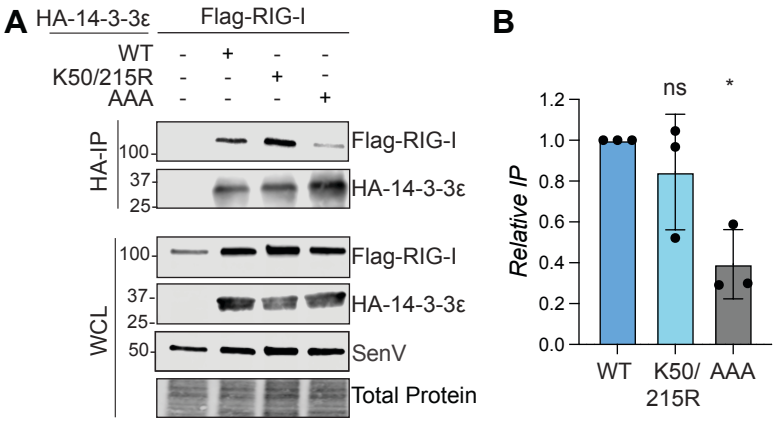

Figure 3. K50 and K215 are not required for 14-3-3ε interaction with RIG-I. (A) Immunoblot analysis of anti-HA immunoprecipitated extracts and inputs from 293T RIG-I KO cells expressing Flag-RIG-I, and HA-14-3-3ε WT, K50/215R, or AAA. Representative blot from $n = 3$ independent replicates is shown. (B) Relative quantification of the ratio of RIG-I (IP/relative input) to immunoprecipitated 14-3-3ε is shown on the right (Mean ± SD, $n = 3$). *$p \leq 0.05$ or non-significant (ns) determined by one way ANOVA followed by Tukey's multiple comparisons test.

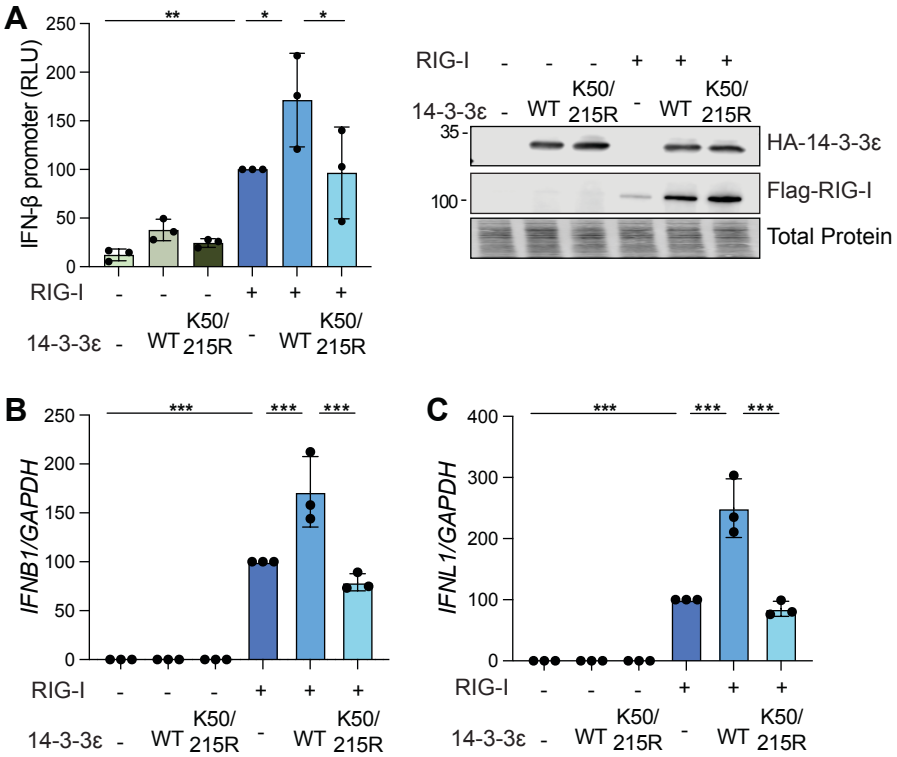

Figure 4. K50 and K215 are required for 14-3-3ε-mediated RIG-I activation of IFN. (A) IFN-β-promoter reporter luciferase expression from 293T RIG-I KO cells expressing Vector (-), Flag-RIG-I, and HA-14-3-3ε^{WT} or HA-14-3-3ε$^{K50/215R}$, with RIG-I samples normalized to 100. (B-C) RT-qPCR analysis (rel. to *GAPDH*) of RNA extracted from 293T RIG-I KO cells transfected with Flag-RIG-I, and HA-14-3-3ε^{WT} or HA-14-3-3ε$^{K50/215R}$ followed by Sendia virus infection (6 h), with RIG-I samples normalized to 100. *p ≤ 0.05, ** ≤ 0.01, ***p ≤ 0.005 determined by one way ANOVA followed by (A) Bonferroni or (B-C) Tukey's multiple comparisons test. Mean ± SD, n = 3 independent replicates are shown.

297 **Methods**

298 **Cell lines, viruses, and transfection.** 293T, 293T-UFM1 KO, and 293T-RIG-I KO were grown
299 in Dulbecco's modification of Eagle's medium (DMEM; Mediatech) supplemented with 10% fetal
300 bovine serum, 1X minimum essential medium nonessential amino acids, and 25 mM of HEPES
301 buffer. The 293T cells (CRL-3216) were obtained from American Type Culture Collection (ATCC).
302 293T-UFM1 KO and 293T-RIG-I KO were previously described (20, 60). All cell lines were verified
303 as mycoplasma-free using the Look-Out Mycoplasma PCR detection kit (Sigma-Aldrich). Sendai
304 virus Cantell strain was obtained from Charles River Laboratories and used at 200 HAU/ml.
305 Sendai virus infections were performed in serum-free media (30 to 60 mins), after which complete
306 medium was added. DNA transfections were performed using FuGene 6 (Promega). Cells were
307 incubated for 24-48 hours post transfection prior to experimental treatment.

308

309 **Plasmids.** The following plasmids have been previously described: pIFN-β-luc (61), pCMV-
310 Renilla (Promega), pcTak_Myc-5_UFL1 (20), pETDuet-His$_6$-TEV-UFL1-StrepII-3C-UFBP1$^{(21\text{-end})}$
311 (gift of Dr. Yogesh Kulathu) (28), pTRIPZ IFNB1^{2x}-Gluc (gift of Dr. Nandan Gokhale) (60), and
312 pET-NT*-HRV3CP (gift of Dr. Gottfried Otting; Addgene #162795) (55). The following plasmids
313 were generated by insertion of PCR-amplified fragments into NotI-to-PmeI digested pEF-TAK-
314 Flag or into BamHI-to-NotI digested pGEX-GST using InFusion cloning (Takara): pGEX-GST-14-
315 3-3ε^{WT}, pGEX-GST-14-3-3ε$^{K50/215R}$, pGEX-GST-UBA5, pGEX-GST-UFC1, and pGEX-GST-
316 UFM1. The following plasmids were generated by site-directed mutagenesis: pEF-TAK-HA-14-3-
317 3ε$^{K50/215R}$, pEF-TAK-HA-14-3-3ε^{AAA} (E251-253A), and pEF-TAK-Flag-UFM1$^{\Delta C2}$. The following
318 were cloned by InFusion: pEF-TAK-Flag-UFM1^{WT}, pEF-TAK-Flag-UFM1$^{\Delta C3}$, and pEF-TAK-Flag-
319 UFM1 G83A from pEF-TAK-HA-UFM1 (20); pEF-TAK-Flag-RIG-I from pEF-Bos-Flag-RIG-I (62),
320 pEF-TAK-HA-14-3-3ε^{WT} from pEF-TAK-Flag-14–3-3ε (20), and pEF-TAK-Myc-UFBP1 by PCR
321 from BC115617. Plasmid sequences were verified by DNA sequencing.

322

323 **IFN-β promoter luciferase assay.** IFN-β promoter luciferase assays were performed at 18 to 24
324 hours after treatment and transfection of pIFN-β-luc and pCMV-Renilla by using the Dual-
325 Luciferase Reporter System (Promega). *Firefly* luciferase was normalized to *Renilla* luciferase,
326 whose expression is driven by the CMV promoter. For the *Gaussia* luciferase assays, 48 hours
327 post transfection of pTRIPZ IFNB1^{2x}-Gluc, supernatant was assayed for *Gaussia* luciferase using
328 the *Renilla* Luciferase Assay System (Promega). All samples were read using a BioTek Synergy2
329 microplate reader.

330

331 **Immunoblotting.** Cells were lysed with either RIPA (10 mM tris HCl pH [7.5], 150 mM NaCl, 0.5%
332 sodium deoxycholate, and 1% Triton X-100 or NP-40 Lysis Buffer (20 mM Tris HCl [pH 7.4], 100
333 mM NaCl, 0.5% NP-40) supplemented with protease inhibitor mixture (Sigma-Aldrich), and Halt
334 inhibitor phosphatase (Thermo Fisher Scientific), and lysates were isolated by centrifugation.
335 Quantified protein was resolved by SDS/PAGE and transferred to nitrocellulose membranes.
336 Membranes were stained with Revert 700 total protein stain (Li-COR Biosciences) and then
337 blocked with 3% bovine serum albumin in phosphate-buffered saline containing 0.01% Tween-
338 20 (PBS-T). Following incubation with primary antibodies, membranes were incubated with
339 species-specific horseradish-peroxidase (HRP)-conjugated antibodies (Jackson Immuno
340 Research 1:5000), followed by membrane treatment with Clarity Western ECL substrate (Bio-
341 Rad) and imaging on a LICOR Odyssey FC. The following antibodies were used for
342 immunoblotting: R-anti-SenV (MBL, 1:1000), HA-HRP (Sigma-Aldrich 1:1000-1:3000), Flag-HRP
343 (1:1000-1:5000), and M-anti-Myc (Cell Signaling Technology 1:1000).
344
345 **Protein immunoprecipitation.** Cells were lysed with either RIPA (10 mM tris HCl [pH 7.5], 150
346 mM NaCl, 0.5% sodium deoxycholate, and 1% triton X-100 or NP-40 Lysis Buffer (20 mM Tris
347 HCl [pH 7.4], 100 mM NaCl, 0.5% NP-40) supplemented with protease inhibitor mixture (Sigma-
348 Aldrich), and Halt phosphatase inhibitor, and 10% glycerol. Quantified protein (between 100-200
349 µg) was incubated anti-HA magnetic beads (Invitrogen) in lysis buffer either at room temperature
350 for 1-2 hrs or 4°C overnight with head-over-tail rotation. Beads were washed 3X in lysis buffer
351 and eluted with 2X Laemmli buffer (Bio-Rad) with 5% 2-mercaptoenthanol at 95°C for 5 minutes.
352 Proteins were resolved by SDS/PAGE and immunoblotting, as above. For UFMylation
353 precipitations, cells were lysed UFMylation lysis buffer (50 mM Tris [pH 8], 150 mM NaCl, 0.5%
354 sodium deoxycholate, and 1% NP-40) supplemented with 10% glycerol, 1:100 protease and
355 phosphatase inhibitors, as above, and 1:100 *N*-ethylmaleimide (10 mM final) (Sigma-Aldrich).
356 Post-nuclear lysates were boiled at 95°C for 10 mins and incubated with Pierce anti-HA magnetic
357 beads with UFMylation lysis buffer. Beads were washed 3X in high salt buffer (10 mM Tris [pH 8],
358 1 mM EDTA, 500 mM NaCl) and eluted with 2X Laemmli buffer with 5% 2-mercaptoenthanol at
359 95°C for 5 minutes.
360
361 **Quantification of immunoblots.** Immunoblots were imaged using the LICOR Odyssey FC
362 system and quantified using ImageStudio software, and raw values were normalized to relevant
363 controls for each antibody. RIG-I and 14-3-3ε interaction were quantified as ratio of inputs of RIG-

364 I and 14-3-3ε normalized to total protein and displayed as the relative ratio of RIG-I over 14-3-3ε
365 pull down.
366
367 **Purification of GST/His-tagged proteins.** pGEX-GST-UBA5, pGEX-GST-UFC1, pGEX-GST-
368 UFM1, pGEX-GST-14-3-3ε, pGEX-GST-14-3-3ε K50/215R, and pETDuet-His_6-TEV-UFL1-
369 StrepII-3C-UFBP1$^{(21\text{-end})}$ were transformed in *E. coli* Rosetta cells. Cells were cultured at 37°C
370 until OD600 reached 0.6 to 0.8. Then, cells were induced with a final concentration of 1 mM IPTG.
371 Cells were further cultured at 30°C for 3.5-4 hours. Cells were collected by centrifugation for 30
372 mins at 7,000 rpm. The pellets were lysed in NET--N buffer (50 mM Tris-HCl [pH 7.5], 150 mM
373 NaCl, 0.5% IGEPAL, supplemented with Aprotinin, Leupeptin, PMSF, and dithiothreitol (DTT) at
374 1:100. Cells were sonicated 3 times for 30 sec at output 6-7 and a duty cycle of 80%. Then,
375 lysates were centrifuged for 30 mins at 12,000 rpm at 4°C. Supernatant was incubated with GST
376 beads that were washed with NETN buffer with rotation at 4C for 1-2 hours. The beads were
377 washed 3 times with NETN buffer and 3 times with PBS supplemented with 1:100 DTT. After
378 washes, GST tag was cleaved with purified human rhinovirus 3C protease (purified as described
379 (55)) and protein was eluted with PBS by incubation with rotation at 4°C overnight.
380
381 ***In vitro* UFMylation.** 2 μM of substrate, 0.25 μM of UBA5, 5 μM UFC1, 20 ng UFL1/UFBP1, 30
382 μM UFM1 were incubated in a reaction buffer containing 50 mM HEPES [pH 7.5], 10 mM $MgCl_2$,
383 with or without 5 mM ATP for 1 hr at 37°C. The reaction was stopped by the addition of 2X SDS
384 loading with 5% 2-mercaptoethanol and incubated at 95°C for 5 minutes The reaction products
385 were then separated by SDS/PAGE and analyzed by immunoblotting, as above.
386
387 **RNA Analysis.** Total cellular RNA was extracted using RNeasy Plus mini kit (Qiagen). RNA was
388 then reverse transcribed using iScript complementary DNA (cDNA) synthesis kit (Bio-Rad),
389 following manufacturer's instructions. The resulting DNA was diluted 1:3 in double distilled water.
390 RT-qPCR was performed in triplicate using the Power SYBR Green PCR master mix (Thermo
391 Fisher Scientific) and QuantStudio 6 Flex RT-PCR system. Oligonucleotide sequences are as
392 follows: IFNB1 F-5'-CTTTGCTATTTTCAGACAAGATTCA; R-5'GCCAGGAGGTTCTCAACAAT,
393 IFNL1 F-5'-CTTCCAAGCCCACCACAACT; R-5'-GGCCTCCAGGACCTTCAGC, and
394 GAPDH F-5'-AAGGTGAAGGTCGGAGTCAAC; R-5'-GGGGTCATTGATGGCAACAATA.
395
396 **Sample Preparation and LC-MS/MS Analysis.** Samples were spiked with undigested bovine
397 casein at a total of either 120 or 240 pmol as an internal quality control standard. Next, samples

398 were supplemented with 10 µL of 20% SDS, reduced with 10 mM DTT for 30 min at 80°C,
399 alkylated with 20 mM iodoacetamide for 30 min at room temperature, then supplemented with a
400 final concentration of 1.2% phosphoric acid and 546 µL of S-Trap (Protifi) binding buffer (90%
401 MeOH/100 mM TEAB). Proteins were trapped on the S-Trap micro cartridge, digested using 20
402 ng/µL sequencing grade trypsin (Promega) for 1 hr at 47°C, and eluted using 50 mM TEAB,
403 followed by 0.2% FA, and lastly using 50% ACN/0.2% FA. All samples were then lyophilized to
404 dryness. Samples were resolubilized using 48 µL of 1% TFA/2% ACN with 25 fmol/µL yeast ADH.
405 Quantitative LC/MS/MS was performed on 1.5 µL (3.13% of total sample) using an MClass UPLC
406 system (Waters Corp) coupled to an Orbitrap Fusion Lumos high resolution accurate mass
407 tandem mass spectrometer (Thermo Fisher Scientific) via a nanoelectrospray ionization source.
408 Briefly, the sample was first trapped on a Symmetry C18 20 mm × 180 µm trapping column (5
409 µl/min at 99.9/0.1 v/v water/acetonitrile), after which, the analytical separation was performed
410 using a 1.8 µm Acquity HSS T3 C18 75 µm × 250 mm column (Waters Corp.) with a 90-min linear
411 gradient of 5 to 30% acetonitrile with 0.1% formic acid at a flow rate of 400 nanoliters/minute
412 (nL/min) with a column temperature of 55°C. Data collection on the Fusion Lumos mass
413 spectrometer was performed in a data-dependent acquisition (DDA) mode of acquisition with a
414 r=120,000 (@ m/z 200) full MS scan from m/z 375 – 1500 with a target AGC value of 4e5 ions
415 was performed. MS/MS scans were acquired in the linear ion trap in “rapid” mode with a target
416 AGC value of 1e5 and max fill time of 100 ms. The total cycle time 2s, with total cycle times of 2
417 sec between like full MS scans. A 20s dynamic exclusion was employed to increase depth of
418 coverage. The total analysis cycle time for each sample injection was approximately 2 hours.
419
420 **Proteomics Data Analysis.** Following UPLC-MS/MS analyses, data were imported into
421 Proteome Discoverer 2.5 (Thermo Fisher Scientific). In addition to quantitative signal extraction,
422 the MS/MS data was searched against the SwissProt *H. sapiens* database (downloaded in Nov
423 2019) and a common contaminant/spiked protein database (bovine albumin, bovine casein, yeast
424 ADH, etc.), and an equal number of reversed-sequence “decoys” for false discovery rate
425 determination. Sequest (v 2.5, Thermo PD) was utilized to produce fragment ion spectra and to
426 perform the database searches. Database search parameters included fixed modification on Cys
427 (carbamidomethyl) and variable modification on Met (oxidation) and Lys (UFMylation). Search
428 tolerances were 2ppm precursor and 0.8Da product ion with semi-trypsin enzyme rules.
429 Discoverer were used to annotate the data at a maximum 1% protein false discovery rate based
430 on q-value calculations. Note that peptide homology was addressed using razor rules in which a
431 peptide matched to multiple different proteins was exclusively assigned to the protein has more

432 identified peptides. Protein homology was addressed by grouping proteins that had the same set
433 of peptides to account for their identification. A master protein within a group was assigned based
434 on % coverage.
435
436 **Statistical analysis.** We used one-way ANOVA followed by appropriate multiple comparisons
437 test using GraphPad Prism software. Graphed values are presented as mean ± SD (n = 3); *$P \leq$
438 0.05, **$P \leq 0.01$, and ***$P \leq 0.001$.
439

440 **References**

441 1. Rehwinkel J, Gack MU. 2020. RIG-I-like receptors: their regulation and roles in RNA
442 sensing. Nat Rev Immunol 20:537-551.

443 2. Crow YJ, Stetson DB. 2022. The type I interferonopathies: 10 years on. Nat Rev
444 Immunol 22:471-483.

445 3. Iwasaki A, Medzhitov R. 2015. Control of adaptive immunity by the innate immune
446 system. Nat Immunol 16:343-53.

447 4. Taft J, Bogunovic D. 2018. The Goldilocks Zone of Type I IFNs: Lessons from Human
448 Genetics. J Immunol 201:3479-3485.

449 5. Lin JP, Fan YK, Liu HM. 2019. The 14-3-3eta chaperone protein promotes antiviral
450 innate immunity via facilitating MDA5 oligomerization and intracellular redistribution.
451 PLoS Pathog 15:e1007582.

452 6. Liu HM, Loo YM, Horner SM, Zornetzer GA, Katze MG, Gale M, Jr. 2012. The
453 mitochondrial targeting chaperone 14-3-3epsilon regulates a RIG-I translocon that
454 mediates membrane association and innate antiviral immunity. Cell Host Microbe
455 11:528-37.

456 7. Aitken A. 2011. Post-translational modification of 14-3-3 isoforms and regulation of
457 cellular function. Semin Cell Dev Biol 22:673-80.

458 8. Pennington KL, Chan TY, Torres MP, Andersen JL. 2018. The dynamic and stress-
459 adaptive signaling hub of 14-3-3: emerging mechanisms of regulation and context-
460 dependent protein-protein interactions. Oncogene 37:5587-5604.

461 9. Henriksson ML, Francis MS, Peden A, Aili M, Stefansson K, Palmer R, Aitken A,
462 Hallberg B. 2002. A nonphosphorylated 14-3-3 binding motif on exoenzyme S that is
463 functional in vivo. Eur J Biochem 269:4921-9.

464 10. Ottmann C, Yasmin L, Weyand M, Veesenmeyer JL, Diaz MH, Palmer RH, Francis MS,
465 Hauser AR, Wittinghofer A, Hallberg B. 2007. Phosphorylation-independent interaction
466 between 14-3-3 and exoenzyme S: from structure to pathogenesis. EMBO J 26:902-13.

467 11. Liu J, Cao S, Ding G, Wang B, Li Y, Zhao Y, Shao Q, Feng J, Liu S, Qin L, Xiao Y. 2021.
468 The role of 14-3-3 proteins in cell signalling pathways and virus infection. J Cell Mol Med
469 25:4173-4182.

470 12. Obsilova V, Obsil T. 2022. Structural insights into the functional roles of 14-3-3 proteins.
471 Front Mol Biosci 9:1016071.

472 13. Toleman CA, Schumacher MA, Yu SH, Zeng W, Cox NJ, Smith TJ, Soderblom EJ,
473 Wands AM, Kohler JJ, Boyce M. 2018. Structural basis of O-GlcNAc recognition by
474 mammalian 14-3-3 proteins. Proc Natl Acad Sci U S A 115:5956-5961.

475 14. Segal D, Maier S, Mastromarco GJ, Qian WW, Nabeel-Shah S, Lee H, Moore G,
476 Lacoste J, Larsen B, Lin ZY, Selvabaskaran A, Liu K, Smibert C, Zhang Z, Greenblatt J,

477 Peng J, Lee HO, Gingras AC, Taipale M. 2023. A central chaperone-like role for 14-3-3
478 proteins in human cells. Mol Cell 83:974-993 e15.

479 15. Chan YK, Gack MU. 2016. A phosphomimetic-based mechanism of dengue virus to
480 antagonize innate immunity. Nat Immunol 17:523-30.

481 16. Riedl W, Acharya D, Lee JH, Liu G, Serman T, Chiang C, Chan YK, Diamond MS, Gack
482 MU. 2019. Zika Virus NS3 Mimics a Cellular 14-3-3-Binding Motif to Antagonize RIG-I-
483 and MDA5-Mediated Innate Immunity. Cell Host Microbe 26:493-503 e6.

484 17. Andrews DDT, Vlok M, Akbari Bani D, Hay BN, Mohamud Y, Foster LJ, Luo H, Overall
485 CM, Jan E. 2023. Cleavage of 14-3-3epsilon by the enteroviral 3C protease dampens
486 RIG-I-mediated antiviral signaling. J Virol 97:e0060423.

487 18. Liu J, Qian C, Cao X. 2016. Post-Translational Modification Control of Innate Immunity.
488 Immunity 45:15-30.

489 19. Zhou Y, He C, Wang L, Ge B. 2017. Post-translational regulation of antiviral innate
490 signaling. Eur J Immunol 47:1414-1426.

491 20. Snider DL, Park M, Murphy KA, Beachboard DC, Horner SM. 2022. Signaling from the
492 RNA sensor RIG-I is regulated by ufmylation. Proc Natl Acad Sci U S A
493 119:e2119531119.

494 21. Komatsu M, Chiba T, Tatsumi K, Iemura S, Tanida I, Okazaki N, Ueno T, Kominami E,
495 Natsume T, Tanaka K. 2004. A novel protein-conjugating system for Ufm1, a ubiquitin-
496 fold modifier. EMBO J 23:1977-86.

497 22. Tatsumi K, Sou YS, Tada N, Nakamura E, Iemura S, Natsume T, Kang SH, Chung CH,
498 Kasahara M, Kominami E, Yamamoto M, Tanaka K, Komatsu M. 2010. A novel type of
499 E3 ligase for the Ufm1 conjugation system. J Biol Chem 285:5417-27.

500 23. Komatsu M, Inada T, Noda NN. 2024. The UFM1 system: Working principles, cellular
501 functions, and pathophysiology. Mol Cell 84:156-169.

502 24. Wei Y, Xu X. 2016. UFMylation: A Unique & Fashionable Modification for Life. Genomics
503 Proteomics Bioinformatics 14:140-146.

504 25. Banerjee S, Kumar M, Wiener R. 2020. Decrypting UFMylation: How Proteins Are
505 Modified with UFM1. Biomolecules 10.

506 26. Millrine D, Peter JJ, Kulathu Y. 2023. A guide to UFMylation, an emerging
507 posttranslational modification. FEBS J 290:5040-5056.

508 27. Zhou X, Mahdizadeh SJ, Le Gallo M, Eriksson LA, Chevet E, Lafont E. 2024.
509 UFMylation: a ubiquitin-like modification. Trends Biochem Sci 49:52-67.

510 28. Peter JJ, Magnussen HM, DaRosa PA, Millrine D, Matthews SP, Lamoliatte F,
511 Sundaramoorthy R, Kopito RR, Kulathu Y. 2022. A non-canonical scaffold-type E3
512 ligase complex mediates protein UFMylation. EMBO J 41:e111015.

513 29. Zhang Y, Yan M, Yu Y, Wang J, Jiao Y, Zheng M, Zhang S. 2024. 14-3-3epsilon: a
514 protein with complex physiology function but promising therapeutic potential in cancer.
515 Cell Commun Signal 22:72.

516 30. Liang Z, Ning R, Wang Z, Kong X, Yan Y, Cai Y, He Z, Liu XG, Zou Y, Zhou J. 2024.
517 The emerging roles of UFMylation in the modulation of immune responses. Clin Transl
518 Med 14:e70019.

519 31. Qin B, Yu J, Nowsheen S, Wang M, Tu X, Liu T, Li H, Wang L, Lou Z. 2019. UFL1
520 promotes histone H4 ufmylation and ATM activation. Nat Commun 10:1242.

521 32. Qin B, Yu J, Nowsheen S, Zhao F, Wang L, Lou Z. 2020. STK38 promotes ATM
522 activation by acting as a reader of histone H4 ufmylation. Sci Adv 6:eaax8214.

523 33. Ishimura R, El-Gowily AH, Noshiro D, Komatsu-Hirota S, Ono Y, Shindo M, Hatta T, Abe
524 M, Uemura T, Lee-Okada HC, Mohamed TM, Yokomizo T, Ueno T, Sakimura K,
525 Natsume T, Sorimachi H, Inada T, Waguri S, Noda NN, Komatsu M. 2022. The UFM1
526 system regulates ER-phagy through the ufmylation of CYB5R3. Nat Commun 13:7857.

527 34. Liang JR, Lingeman E, Luong T, Ahmed S, Muhar M, Nguyen T, Olzmann JA, Corn JE.
528 2020. A Genome-wide ER-phagy Screen Highlights Key Roles of Mitochondrial
529 Metabolism and ER-Resident UFMylation. Cell 180:1160-1177 e20.

530 35. Scavone F, Gumbin SC, Da Rosa PA, Kopito RR. 2023. RPL26/uL24 UFMylation is
531 essential for ribosome-associated quality control at the endoplasmic reticulum. Proc Natl
532 Acad Sci U S A 120:e2220340120.

533 36. Walczak CP, Leto DE, Zhang L, Riepe C, Muller RY, DaRosa PA, Ingolia NT, Elias JE,
534 Kopito RR. 2019. Ribosomal protein RPL26 is the principal target of UFMylation. Proc
535 Natl Acad Sci U S A 116:1299-1308.

536 37. Wang L, Xu Y, Rogers H, Saidi L, Noguchi CT, Li H, Yewdell JW, Guydosh NR, Ye Y.
537 2020. UFMylation of RPL26 links translocation-associated quality control to endoplasmic
538 reticulum protein homeostasis. Cell Res 30:5-20.

539 38. Xu X, Huang W, Bryant CN, Dong Z, Li H, Wu G. 2024. The ufmylation cascade controls
540 COPII recruitment, anterograde transport, and sorting of nascent GPCRs at ER. Sci Adv
541 10:eadm9216.

542 39. He C, Xing X, Chen HY, Gao M, Shi J, Xiang B, Xiao X, Sun Y, Yu H, Xu G, Yao Y, Xie
543 Z, Xing Y, Budiarto BR, Chen SY, Gao Y, Lee YR, Zhang J. 2024. UFL1 ablation in T
544 cells suppresses PD-1 UFMylation to enhance anti-tumor immunity. Mol Cell 84:1120-
545 1138 e8.

546 40. Yoo HM, Kang SH, Kim JY, Lee JE, Seong MW, Lee SW, Ka SH, Sou YS, Komatsu M,
547 Tanaka K, Lee ST, Noh DY, Baek SH, Jeon YJ, Chung CH. 2014. Modification of ASC1
548 by UFM1 is crucial for ERalpha transactivation and breast cancer development. Mol Cell
549 56:261-274.

550 41. Zhou J, Ma X, He X, Chen B, Yuan J, Jin Z, Li L, Wang Z, Xiao Q, Cai Y, Zou Y, Cong
551 YS. 2023. Dysregulation of PD-L1 by UFMylation imparts tumor immune evasion and
552 identified as a potential therapeutic target. Proc Natl Acad Sci U S A 120:e2215732120.

553 42. Lee L, Perez Oliva AB, Martinez-Balsalobre E, Churikov D, Peter J, Rahmouni D, Audoly
554 G, Azzoni V, Audebert S, Camoin L, Mulero V, Cayuela ML, Kulathu Y, Geli V, Lachaud
555 C. 2021. UFMylation of MRE11 is essential for telomere length maintenance and
556 hematopoietic stem cell survival. Sci Adv 7:eabc7371.

557 43. Wang Z, Gong Y, Peng B, Shi R, Fan D, Zhao H, Zhu M, Zhang H, Lou Z, Zhou J, Zhu
558 WG, Cong YS, Xu X. 2019. MRE11 UFMylation promotes ATM activation. Nucleic Acids
559 Res 47:4124-4135.

560 44. Kulsuptrakul J, Wang R, Meyers NL, Ott M, Puschnik AS. 2021. A genome-wide
561 CRISPR screen identifies UFMylation and TRAMP-like complexes as host factors
562 required for hepatitis A virus infection. Cell Rep 34:108859.

563 45. Schmidt HM, Sorensen GC, Lanahan MR, Grabowski J, Park M, Horner SM. 2025.
564 UFMylation promotes orthoflavivirus infectious particle production. bioRxiv
565 doi:10.1101/2025.01.09.632082:2025.01.09.632082.

566 46. Yiu SPT, Zerbe C, Vanderwall D, Huttlin EL, Weekes MP, Gewurz BE. 2023. An
567 Epstein-Barr virus protein interaction map reveals NLRP3 inflammasome evasion via
568 MAVS UFMylation. Mol Cell 83:2367-2386 e15.

569 47. Jing J, Yang F, Wang K, Cui M, Kong N, Wang S, Qiao X, Kong F, Zhao D, Ji J, Tang L,
570 Gao J, Cong YS, Ding D, Chen K. 2025. UFMylation of NLRP3 Prevents Its Autophagic
571 Degradation and Facilitates Inflammasome Activation. Adv Sci (Weinh)
572 doi:10.1002/advs.202406786:e2406786.

573 48. Wang X, Li C, Wang Y, Li L, Han Z, Wang G. 2020. UFL1 Alleviates LPS-Induced
574 Apoptosis by Regulating the NF-kappaB Signaling Pathway in Bovine Ovarian
575 Granulosa Cells. Biomolecules 10.

576 49. Cai Y, Zhu G, Liu S, Pan Z, Quintero M, Poole CJ, Lu C, Zhu H, Islam B, Riggelen JV,
577 Browning D, Liu K, Blumberg R, Singh N, Li H. 2019. Indispensable role of the Ubiquitin-
578 fold modifier 1-specific E3 ligase in maintaining intestinal homeostasis and controlling
579 gut inflammation. Cell Discov 5:7.

580 50. Li C, Li L, Chen K, Wang Y, Yang F, Wang G. 2019. UFL1 Alleviates
581 Lipopolysaccharide-Induced Cell Damage and Inflammation via Regulation of the
582 TLR4/NF-kappaB Pathway in Bovine Mammary Epithelial Cells. Oxid Med Cell Longev
583 2019:6505373.

584 51. Balce DR, Wang YT, McAllaster MR, Dunlap BF, Orvedahl A, Hykes BL, Jr., Droit L,
585 Handley SA, Wilen CB, Doench JG, Orchard RC, Stallings CL, Virgin HW. 2021.
586 UFMylation inhibits the proinflammatory capacity of interferon-gamma-activated
587 macrophages. Proc Natl Acad Sci U S A 118.

588 52. Tao Y, Yin S, Liu Y, Li C, Chen Y, Han D, Huang J, Xu S, Zou Z, Yu Y. 2023. UFL1
589 promotes antiviral immune response by maintaining STING stability independent of
590 UFMylation. Cell Death Differ 30:16-26.

591 53. Horner SM, Wilkins C, Badil S, Iskarpatyoti J, Gale M, Jr. 2015. Proteomic analysis of
592 mitochondrial-associated ER membranes (MAM) during RNA virus infection reveals
593 dynamic changes in protein and organelle trafficking. PLoS One 10:e0117963.

594 54. Zhou J, Liang Q, Dong M, Ma X, Jin Y, Guan D, Liu J, Wang M, Cong YS. 2022.
595 Optimized protocol to detect protein UFMylation in cells and in vitro via immunoblotting.
596 STAR Protoc 3:101074.

597 55. Abdelkader EH, Otting G. 2021. NT*-HRV3CP: An optimized construct of human
598 rhinovirus 14 3C protease for high-yield expression and fast affinity-tag cleavage. J
599 Biotechnol 325:145-151.

600 56. Cantell K, Hirvonen S, Kauppinen HL, Myllyla G. 1981. Production of interferon in
601 human leukocytes from normal donors with the use of Sendai virus. Methods Enzymol
602 78:29-38.

603 57. Sumpter R, Jr., Loo YM, Foy E, Li K, Yoneyama M, Fujita T, Lemon SM, Gale M, Jr.
604 2005. Regulating intracellular antiviral defense and permissiveness to hepatitis C virus
605 RNA replication through a cellular RNA helicase, RIG-I. J Virol 79:2689-99.

606 58. Fan K, Zhu K, Wang J, Ni X, Shen S, Gong Z, Cheng X, Zhang C, Liu H, Suo T, Ni X,
607 Liu H. 2022. Inhibition of 14-3-3epsilon by K50 acetylation activates YAP1 to promote
608 cholangiocarcinoma growth. Exp Cell Res 421:113404.

609 59. Hendriks IA, Lyon D, Young C, Jensen LJ, Vertegaal AC, Nielsen ML. 2017. Site-
610 specific mapping of the human SUMO proteome reveals co-modification with
611 phosphorylation. Nat Struct Mol Biol 24:325-336.

612 60. Gokhale NS, Sam RK, Somfleth K, Thompson MG, Marciniak DM, Smith JR, Genoyer E,
613 Eggenberger J, Chu LH, Park M, Dvorkin S, Oberst A, Horner SM, Ong SE, Gale M, Jr.,
614 Savan R. 2024. Cellular RNA interacts with MAVS to promote antiviral signaling.
615 Science 386:eadl0429.

616 61. Fredericksen B, Akkaraju GR, Foy E, Wang C, Pflugheber J, Chen ZJ, Gale M, Jr. 2002.
617 Activation of the interferon-beta promoter during hepatitis C virus RNA replication. Viral
618 Immunol 15:29-40.

619 62. Saito T, Hirai R, Loo YM, Owen D, Johnson CL, Sinha SC, Akira S, Fujita T, Gale M, Jr.
620 2007. Regulation of innate antiviral defenses through a shared repressor domain in RIG-
621 I and LGP2. Proc Natl Acad Sci U S A 104:582-7.
622